Applied Catalysis B: Environmental 154–155 (2014) 386–394

Contents lists available at ScienceDirect

Applied Catalysis B: Environmental

journal homepage: www.elsevier.com/locate/apcatb

Evaluation of Co, La, and Mn promoted Rh catalysts for autothermal reforming of commercial diesel

Moa Z. Granlund[a,*], Kjell Jansson[b], Marita Nilsson[c], Jazaer Dawody[d], Lars J. Pettersson[a]

[a] KTH Royal Institute of Technology, Department of Chemical Engineering and Technology, SE-100 44 Stockholm, Sweden
[b] Stockholm University, Arrhenius Laboratory, Department of Materials and Environmental Chemistry, SE-106 91 Stockholm, Sweden
[c] Scania CV AB, Materials Technology, Engine Performance and Emissions, SE-151 87 Södertälje, Sweden
[d] Volvo Group Trucks Technology, Advanced Technology & Research, Energy Efficiency & Environment, SE-412 88 Göteborg, Sweden

ARTICLE INFO

Article history:
Received 30 November 2013
Received in revised form 18 February 2014
Accepted 22 February 2014
Available online 3 March 2014

Keywords:
Autothermal reforming
Rhodium
Bimetallic
Diesel
Monolith

ABSTRACT

The objective of this paper was to study the influence three promoters (Co, La, Mn) had on the catalytic activity of Rh-based catalysts for autothermal reforming of diesel. The catalysts were supported on CeO_2-ZrO_2 and the loading was 1 wt.% Rh and 6 wt.% promoter. The catalytic activity was evaluated in a monolith bench scale reactor with Swedish Environmental diesel, MK1. The process parameters employed at the ATR experiments were; $O_2/C \sim 0.45$, $H_2O/C \sim 2.5$ and GHSV $\sim 50{,}000\ h^{-1}$, meanwhile the reactor temperature was ramped from 700 °C to 950 °C. The catalysts were compared based on their fuel conversion, H_2 yield and the selectivity of different short-chain hydrocarbons.

The results showed that all three catalysts had both high fuel conversion and H_2 yield in the optimal ATR operation temperatures. The H_2 yield and fuel conversion were increasing in the order Rh/Mn, Rh/La, Rh/Co. To get further insight in the difference between the materials the fresh and aged catalytic materials were characterized. The characterization methods used were H_2-temperature programmed reduction (H_2-TPR), powder X-ray diffraction (XRD), and BET surface measurements. The BET surface measurements showed that promotion with La gave improved thermal stability of the material. The XRD showed a high dispersion of all metals except Co, which was present as crystals in the size range of the particles of the support.

1. Introduction

Hydrogen is one of the more promising candidates for replacing fossil fuels in the future in both stationary and mobile applications. In mobile applications hydrogen can be used both as propellant, supplementary fuel and as an additive to increase the performance of different applications. For heavy duty diesel vehicles (HDDVs), hydrogen is an attractive option both as supplementary fuel, as fuel for a fuel cell auxiliary power unit (FC APU), and additive in various applications. The applications where hydrogen can be used as additives are many: (i) enhancing the low-temperature lean NO_x catalyst activity [1], (ii) regeneration of the NO_x trap catalyst, (iii) heating the after-treatment system to minimize the start-up time, (iv) reducing the NO_x formation in the engine [2].

Among these areas the use of an FC APU is the most attractive option since it would significantly lower the emissions and fuel consumption during stand-stills [3–5]. It is estimated that an HDDV is idling on average 6 h per day for 290 days annually in order to provide the vehicle with electricity for cabin comfort [6]. The emission during idling is approximately 10% of the total emissions [7]. Using a FC APU as power generator during standstills would also mean less wear of the engine and prolong its life time [8,9].

One of the main problems connected to the usage of hydrogen in mobile applications is its low energy density in gas phase, making the storage an issue. Today, there are several options available for onboard storage of hydrogen (a) pressurized gas, (b) cryogenic liquid, (c) solid fuel e.g. metal hydrides or (d) onboard production from hydrocarbon based fuels (diesel, methanol, etc.) via reforming [10]. To introduce hydrogen onboard vehicles onboard reforming is considered as an attractive alternative. The main advantage with reforming diesel as hydrogen source is the already existing and well-expanded infrastructure [11]. It is also an advantage to use the propellant as hydrogen storage to avoid having two different fuel tanks on the vehicle. In order to retrieve the hydrogen stored in the fuel it is reformed in a fuel processor.

There are three available reforming processes: partial oxidation (POX), steam reforming (SR) and autothermal reforming (ATR). There are advantages and disadvantages with all three reforming

* Corresponding author. Tel.: +46 8 790 9150.
E-mail address: moazg@kth.se (M.Z. Granlund).

http://dx.doi.org/10.1016/j.apcatb.2014.02.043
0926-3373/

schemes that need to be considered when choosing the most suitable scheme for the current application. For remote applications where water supply is limited POX is the most attractive alternative since there is no need for steam. The lack of steam in POX makes the process highly sensitive to coking. The benefits with POX are the fast thermal response and that the process is highly exothermic [12]. SR is a strongly endothermic reaction and needs water as reactant. This causes the SR process to have a more complex reactor set-up than the other two available options. However SR has the highest H_2 yield of the three reforming processes. [13] ATR is a combination of POX followed by SR, giving the ATR reaction the benefits of fast thermal response and high H_2 yield. The fact that both oxygen and steam is present in the reactant mixture is a great advantage when reforming commercial fuel. The oxygen contributes to a fast pre-reforming of the diesel making it easier to steam reform. The added steam makes sure that coke on the catalyst surface in the beginning of the reactor is limited. Additionally, ATR requires no external heating. This makes ATR a suitable reaction for generating H_2 from fuel onboard HDDVs. [14]

ATR of both light and heavy hydrocarbons (HCs) has been studied extensively over the years. Traditionally for heavy HC, i.e. transport fuel, the best choice is considered to be platinum group metals (PGM) supported on alumina [15]. Among the PGMs, Rh is considered to be the best option due to its excellent C—C bond cleavage properties. Alumina is used for its high thermal resistance and high specific surface area, which are two key parameters for good support in a catalyst material [16]. The two main drawbacks of using alumina are the acidity of the material, which may lead to extensive coking of the catalyst and eventually catalyst failure, and the fact that the transition between the different crystal phases is in the optimal temperature range for ATR. To minimize the effect of these drawbacks, CeO_2 and La_2O_3 are added to the catalyst. The addition of CeO_2 suppresses the coke formation and also keeps the PGM in a more dispersed state [17]. By adding La_2O_3 to the alumina, the phase stability is enhanced [16].

The first thing was to choose a suitable support material for the catalytic material. In this work, CeO_2-ZrO_2 was chosen as support for the material, based on previous work done in our laboratory showing that CeO_2-ZrO_2 is a more suitable support then alumina for ATR of diesel [18,19]. The main reason was concluded to be the high transportation of bulk oxygen in CeO_2-ZrO_2, enhancing the oxidation of coke formed on the surface and thereby prolonging the lifetime of the catalytic material. Moreover, CeO_2 is the most basic oxide and therefore able to quench the coke formation; however, basicity decreases with increasing ZrO_2 content [20]. These properties of CeO_2-ZrO_2 have proven to be advantageous in many other applications [21] such as catalytic combustion of hydrocarbons [22], photocatalytic applications [23], and removal of pollutants in water [24].

It is proven that the catalytic activity for ATR of diesel increases with increased Rh loading [19]. However, the PGM metals are expensive and the resources are limited at the same time as the demand increases [25]. Therefore there is a need to find catalytic materials for ATR with a lower amount of PGM metal, but with retained catalytic activity and stability. The scope of this article is to investigate whether the catalytic activity of a 3 wt.% Rh/CeO_2-ZrO_2 catalyst can be reached with a 1 wt.% Rh/6 wt.% promoter/CeO_2-ZrO_2 catalyst. Three promising promoters were chosen (Co, La, and Mn) and the catalysts were prepared with 1 wt.% Rh and 6 wt.% promoter.

The three promoters were chosen based on previously reported results in the field or adjacent fields. Mn has been reported to enhance the oxygen storage capacity (OSC) of three-way catalysts compared to having CeO_2 alone and to enhance the water-gas shift (WGS) activity of the catalyst [26,27]. Furthermore, Rh/Mn has been shown by Nilsson [19] to be a promising candidate for ATR of diesel. La was chosen since CeO_2-ZrO_2 promoted with La has been reported to have high H_2 yield and low HC selectivity together with high resistance towards coking [28]. The combination of Rh and Co has been shown in other studies to have high activity for reforming of higher HC and to favor the selectivity for H_2 due to the strong metal interaction between the species. This strong interaction between Rh and Co could suppress the volatility of Co under the harsh ATR reaction conditions. Co is known to coke easily; however, in combination with Rh this property is suppressed due to the high C–C cleavage activity of Rh [29].

This article is the first of two articles evaluating cobalt's, lanthanum's and manganese's potential to replace part of the Rh content in diesel ATR catalysts without sacrificing the catalytic activity. The evaluated catalysts are 1 wt.% Rh/6 wt.% X (X = Co, La, Mn) supported on CeO_2-ZrO_2. The first article covers catalytic activity and basic characterization (XRD, surface area measurements, and H_2-TPR) and the second part covers deactivation and further characterization (TPO, TEM, SEM, CO chemisorption, H_2-TPR, O_2 pulse chemisorption). The catalytic activity and deactivation was evaluated in a monolithic bench-scale reactor with Swedish Environmental Class 1 diesel, MK1. The process parameters employed at the ATR experiments were; $O_2/C \sim 0.45$, $H_2O/C \sim 2.5$ and GHSV $\sim 50{,}000\ h^{-1}$ meanwhile the reactor temperature was ramped from 700 °C to 950 °C in 50 °C steps.

2. Experimental

2.1. Catalyst preparation

The catalytic materials were prepared by the incipient wetness method. The support used was CeO_2-ZrO_2 with high specific surface area (16.5 wt.% CeO_2, ($Ce_{0.12}O_2Zr_{0.88}O_2$), MEL Chemicals). The metal precursors used were Rh nitrate solution ($Rh(NO_3)_3$, 9.53 w/w, Sigma-Aldrich), Co nitrate ($Co(NO_3)_2{\cdot}6H_2O$, Alfa Aesar), La nitrate ($LaNO_3)_3{\cdot}6H_2O$, Alfa Aesar), and Mn nitrate ($Mn(NO_3)_2{\cdot}xH_2O$, Alfa Aesar).

The metal precursors were separately dissolved and diluted in ultra-pure water. The volume of each metal salt solution was approximately twice the pore volume of the support. The metal salt solutions were then carefully dripped onto the support, the promoter solution followed by the Rh solution, until saturation point was reached. Between each impregnation, the catalyst powders were dried at 110 °C for 3 h. The resulting catalyst powders were calcined in air at 800 °C for 3 h. The calcined catalytic powders were then suspended in ethanol (approximately 16 wt.% dry weight) and ball milled for a minimum of 24 h. The structural support used was honeycomb cordierite monoliths (Corning Celcor®, 400 cpsi, Ø = 20 mm, *l* = 30 mm) on which the catalyst powders were applied by dip coating. The monolith was dipped in the slurry until the catalyst loading was approximately 20 wt.%. Between each dip, the monoliths were carefully dried in pressurized air and then placed at 110 °C for 45 min. After the coating, the monoliths were calcined again in air at 800 °C for 3 h. An overview of the catalytic materials included in the study can be seen in Table 1.

2.2. Characterization of catalytic materials

The catalyst samples were characterized by powder X-ray diffractogram (XRD), surface area measurements and H_2-temperature programmed reduction (H_2-TPR). To be able to analyze the aged catalytic materials it was carefully removed from the monoliths, trying to get as little as possible of the cordierite material in the powder.

XRD measurements on the fresh samples were carried out in a Siemens D5000 diffractometer using a monochromatic Cu Kα

Table 1
Overview of the materials used in the evaluation. All the catalytic materials are supported on high surface-area CeO_2-ZrO_2. The specific surface area was measured after the final calcination at 850 °C and after thermal treatment at 950 °C in air. The thermal treatment is supposed to mimic the initial treatment in the reactor, where the thermal aging is accelerated before the activity tests.

Sample	Fresh samples			Thermally treated samples		
	S_{BET} (m^2/g)	Pore volume (cm^3/g)	Average pore diameter (nm)	S_{BET} (m^2/g)	Pore volume (cm^3/g)	Average pore diameter (nm)
CeO_2-ZrO_2	66.8	0.20	11.9	51.7	0.17	12.9
Rh(1)Co(6)[b]	26.7	0.19	27.4	20.7	0.18	35.0
Rh(1)La(6)[b]	84.6	0.22	10.8	71.3	0.20	16.6
Rh(1)Mn(6)[b]	49.5	0.21	17.2	28.9	0.15	21.5

[b] The numbers in parentheses are the nominal loading (wt.%) of Rh and promoters.

radiation source (30 mA, 40 kV). The intensities were acquired in the range 10–90° with a step size of 0.02° and sampling time of 6 s. X-ray diffraction patterns of the aged samples were recorded with a PANalytical Xpert PRO MPD diffractometer using a Cu Kα radiation (30 mA, 45 kV), variable slits with constant area of 1 cm^{-2} radiated and step size of 0.0167°. Intensities were recorded in the 2θ range 20–110°, with a total sample time of 145 min (corresponding to 1.6 s/measuring point). The crystal size of the species that could be detected was calculated by the Scherrer formula for both fresh and aged samples.

The BET specific surface area measurements of the fresh and thermally treated catalytic materials were performed by nitrogen adsorption at the temperature of liquid nitrogen, using an ASAP 2010 from Micromeritics. Prior to the analysis, the catalytic samples were degassed at 250 °C. The thermally treated materials were treated at 950 °C for 30 min in order to investigate the changes in pore structure, depending on temperature.

H_2-TPR experiments were conducted in an Autochem 2910, Micromeritics, equipped with a continuous thermal conductivity detector. Prior to the experiments, the catalytic samples were pre-treated in helium at 950 °C for 30 min. The H_2-TPR was performed in 5 vol.% H_2/Ar (30 cm^3/min) meanwhile the temperature was raised from ambient to 950 °C (10 °C/min). H_2-TPR analyses were performed on the catalytic materials and on the support impregnated with the promoters.

3. ATR activity experiments

The ATR experiments were performed in a horizontally mounted steel monolith reactor (Sandvik 253 MA, $Ø_{inner}$ = 24.3 mm). The gas flows (synthetic air and N_2) were controlled by mass flow controllers (Bronkhorst®, El-Flow), the liquid fuel flow by a Coriolis mass flow controller (Bronkhorst®, Mini Cori-Flow) and the deionized water with a continuously operating syringe pump (WPI, Aladdin). The N_2 and synthetic air were mixed and heated prior to the introduction of water. The water was evaporated and mixed with the hot gases in a static mixer (SMX DN4, Sulzer). The steam-air-N_2 mixture flow then enters the fuel vaporization chamber, into which the fuel is sprayed by a N_2-assisted high-pressure nozzle, facilitating the evaporation of the fuel. The reactant mixture is then introduced into the reactor, surrounded by a furnace regulating the temperature. To avoid fuel slip, the monolith is wrapped in ceramic tape prior to mounting it in the reactor. The temperature is measured before and after the monolith. To protect the thermocouples from radiation heat un-coated cordierite monoliths were placed before and after the coated monolith (l = 30 mm, $Ø$ = 20 mm).

The product gases were analyzed with an FTIR instrument, a mass spectrometer and a gas chromatograph (GC). The FTIR instrument (MKS Instruments, Multigas™ 230 *HS*) was equipped with a high-speed spectrometer and analyzing the concentration of H_2O, CO, CO_2, CH_4, light HCs (C_2–C_3) and heavy HCs (C_{4+}) (summarized as a diesel fraction). The GC (Varian CP-3800) was equipped with a thermal conductivity detector and two sequentially packed columns, a Porapak and a molecular sieve (5 Å), and analyzed the H_2, CO_2, O_2, N_2 and CO content of the dry reformate. The mass spectrometer (V & F Instrument Inc., H-sense) analyzed the concentration of H_2 in the dry reformate. The scheme over the complete monolith bench scale reactor set-up can be seen in Fig. 1.

Table 2
Specifications for the low-sulfur diesel (Swedish Environmental Class 1, MK1) [46] and biodiesel (NExBTL) [47] used in the ATR experiments.

Properties	MK1	NExBTL, Neste	Unit
Sulfur content	<10	<1	ppm (w)
Cetane no.	>51	75.8	–
Min. boiling point	180	209	°C
Dist. 95% evap.	<340	293	°C
Aromatics	<5	<0.2	vol.%
RME[2]	<7	–	vol.%

[1] Polycyclic aromatic hydrocarbon.
[2] Rapeseed methyl ester.

Prior to the ATR experiments, the catalysts were pre-treated in N_2, while the temperature was ramped from ambient to 950 °C with a heating rate of 10 °C/min and maintained for 30 min. The procedure was performed to accelerate the initial thermal aging. During the ATR experiments, the gas hourly space velocity (GHSV) was approximately 50,000 h^{-1}, steam-to-carbon ratio (H_2O/C) ~ 2.5 and oxygen-to-carbon ratio (O_2/C) ~ 0.45. The evaluated temperature range was 700–950 °C. Prior to the comparative measurements the catalytic materials were subjected to 4 repeated cycles, approximately 20 h on stream, in order to obtain stable catalytic materials. The fuel used was commercially available Swedish Environmental class 1 diesel (MK1) and commercial biodiesel, NExBTL; see Table 2 for fuel specifications.

3.1. Product analysis and calculations

In the calculations, the diesel is approximated to $C_{14}H_{26}$. The fuel conversion is defined as the amount of C_1 in the diesel that is converted to CO, CO_2 and CH_4 according to Eq. (1):

$$X_{fuel}(\%) = \frac{F_{CO_2} + F_{CO} + F_{CH_4}}{14 \cdot F_{fuel}} \cdot 100 \quad (1)$$

The H_2 yield is defined as the percentage of the theoretical, maximum amount of H_2 formed, assuming that the only products were CO_2 and H_2, i.e. all CO is converted to CO_2 through the WGS reaction:

$$Y_{H_2}(\%) = \frac{F_{H_2} + F_{CO}}{F_{H_2.max}} \cdot 100 \quad (2)$$

The selectivity for CO_2 compared to CO is calculated according to Eq. (3):

$$S_{CO_2}(\%) = \frac{F_{CO_2}}{F_{CO_2} + F_{CO}} \cdot 100 \quad (3)$$

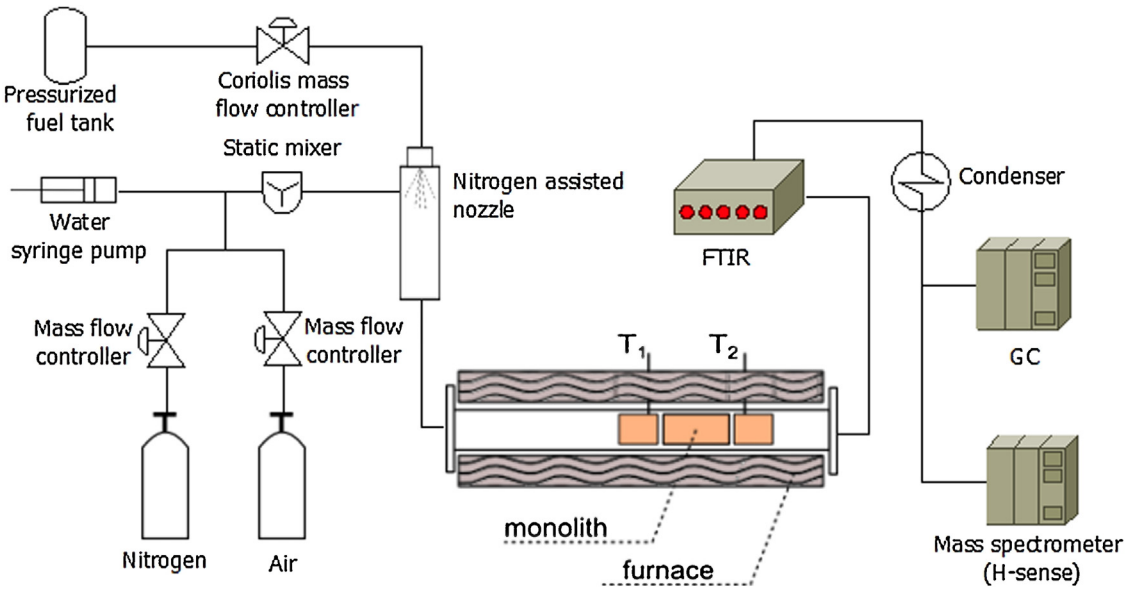

Fig. 1. Scheme over the complete reactor set-up used for the ATR experiments.

The selectivity for the different HC is shown in Eq. (4):

$$S_{C_xH_y} = \frac{y \cdot F_{C_xH_y}}{F_{C_{1,\text{total}}}} \quad (4)$$

The diesel slip is defined as the selectivity of diesel equivalents measured by the FTIR instrument.

4. Results and discussion

4.1. ATR activity experiments

In Fig. 2 the fuel conversions for the three promoted catalytic materials are compared with the fuel conversion of a 3 wt.% Rh catalyst. It can be noticed that all three of the evaluated catalysts have fuel conversion above 80% when the reactor temperature exceeds 800 °C, even though a higher GHSV than normally used in the field is employed. Based on thermodynamic calculations

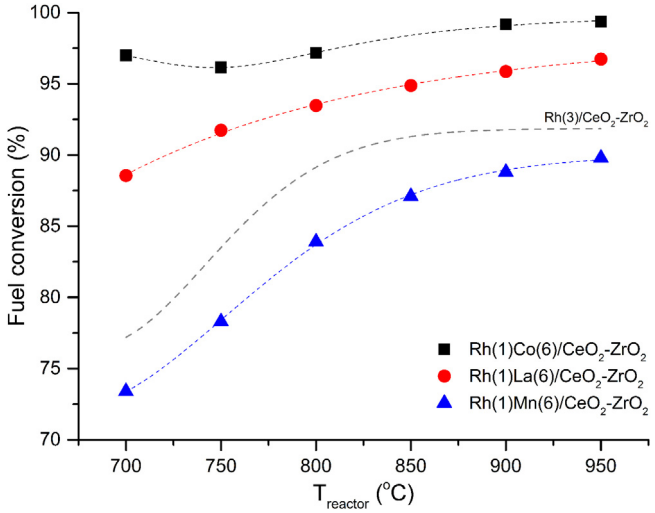

Fig. 2. Comparison of the fuel conversion for the three catalytic samples. The operational parameters during the ATR experiments were GHSV ~ 50,000 h^{-1}, $H_2O/C \sim 2.5$ and $O_2/C \sim 0.45$. The numbers in parenthesis denote the nominal loading (wt.%) of Rh and promoters. The dashed line represents data for a $Rh(3)/CeO_2$-ZrO_2 reforming catalyst performed at the same operational parameters.

the optimal temperature range for ATR of diesel is 750–850 °C [19]. The catalyst with the higher Rh loading is evaluated in the same reactor, at the same operating conditions using commercial biodiesel (NExBTL, Neste Oil). This particular biodiesel, containing very low concentrations of aromatics and sulfur, is easier to reform and less demanding for the catalyst. Therefore the performance of the catalyst with higher Rh loading is overestimated compared to the evaluated promoted catalysts. As can be observed in Fig. 2, the fuel conversions of the evaluated catalysts are comparable with the catalyst with the higher Rh loading. This is in line with previous observations made by our group where catalytic materials with higher Rh loading have been used for reforming [19,30]. This proves that it is possible to lower the Rh content by two thirds (1 wt.% Rh instead of 3 wt.% Rh) by choosing suitable material combinations and maintain the catalytic activity of the material.

Although all three materials evaluated in this study show high fuel conversion, the Rh/Co sample is superior to the other two materials, with a fuel conversion above 95% even at lower reactor temperatures. For the Rh/Mn sample, the fuel conversion is lower than for the other two samples and more dependent on the temperature and, furthermore, does not reach the region where the mass transport is the limiting factor until 900 °C. This can be linked to the fact that the Rh/Mn sample has lower oxygen conversion compared to the other two samples over the whole temperature range. The oxygen conversion for Rh/La and Rh/Co is completed over the whole range, while the oxygen conversion for Rh/Mn never reaches completion, not even at the highest temperatures. This could be an indication that Rh/Mn is not as good a POX catalyst as the other two catalysts.

The fact that the fuel conversion for the Rh/Co sample is almost independent of temperature suggests a faster kinetics for this material. On the other hand both Rh/La and Rh/Mn seem to be kinetically controlled at the lower temperatures.

The dip in fuel conversion at 750 °C for the Rh/Co sample correlates with the point where CO becomes the dominant product in the reformate. The CO_2 selectivity compared to CO is shown in Fig. 3. The shift between CO_2 and CO is most likely the temperature where the steam reforming activity becomes the more dominating reaction. For the lower temperatures where CO_2 is dominating it is likely that there is some water gas shift activity. From the shift in CO_2 selectivity one can conclude that the Rh/Co sample is active for steam reforming at a lower temperature than the other two

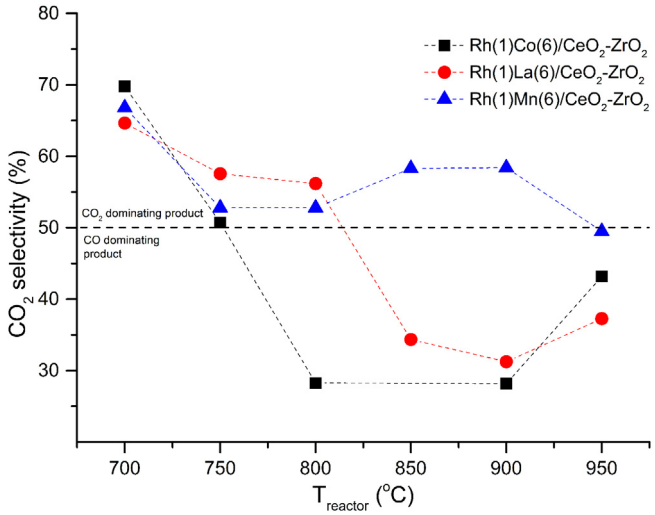

Fig. 3. CO_2 selectivity compared to CO as a function of the reactor temperature. The operational parameters during the ATR experiments were GHSV ~ 50,000 h^{-1}, $H_2O/C \sim 2.5$ and $O_2/C \sim 0.45$. The numbers in parenthesis denote the nominal loading (wt.%) of Rh and promoters.

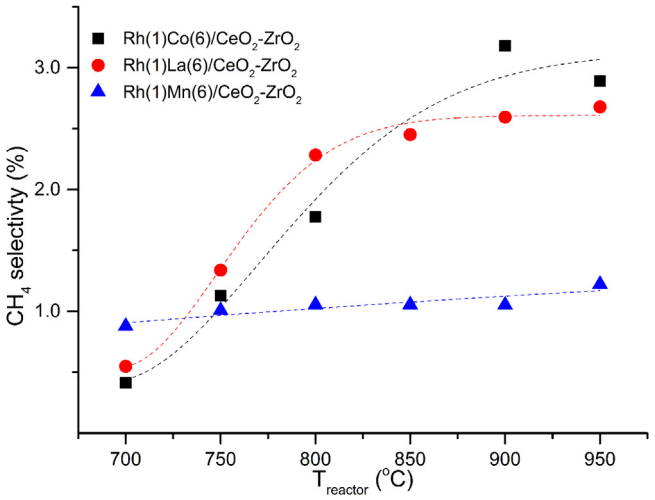

Fig. 5. CH_4 selectivity for the three catalytic materials as a function of the reactor temperature. The operational parameters during the ATR experiments were GHSV ~ 50,000 h^{-1}, $H_2O/C \sim 2.5$ and $O_2/C \sim 0.45$. The numbers in parenthesis denote the nominal loading (wt.%) of Rh and promoters.

materials. For the Rh/Mn sample CO does not become the dominating product, implying that the material is not as good steam reforming catalyst as the Rh/Co and Rh/La samples.

For the Rh/La sample there is evidence, supporting that the steam reforming controls the CO_2 selectivity. The first evidence is the H_2 yield and the other is that the CO_2 selectivity decreases with increased water consumption.

In Fig. 4 the H_2 yields of the catalytic materials are presented. In the figure it is shown that the H_2 yield for the Rh/Co is unaffected by the reactor temperature. The Rh/La sample reaches the same H_2 yield as the Rh/Co sample when the temperature approaches 850 °C. The Rh/Mn sample has a lower H_2 yield than the other two samples throughout the temperature range.

Even though the main products in ATR of diesel are H_2, CO_2, CO, and H_2O, the complexity of diesel, the high number of both catalytic and homogenous reactions involved, and high temperatures, result in the formation of many different by-products, especially short chain HCs. The dominating lighter HCs formed are CH_4 and ethene. The formation of these species is highly unwanted since it decreases the H_2 yield and ethene is also a potential source of coke and eventually catalyst failure [31,32]. Both compounds can be formed as a byproduct from the involved catalytic reaction but can also be formed homogeneously, cracking products. Both CH_4 and ethene start to form homogenously after 700 °C.

The selectivity for CH_4 for the catalytic materials is shown in Fig. 5. The results reveal that the Rh/Mn sample has a much lower selectivity for CH_4 than the other two samples at the optimal ATR temperature range. Additionally, the Rh/Mn sample shows an independency of reactor temperature. The Rh/Mn sample's selectivity for CH_4 is lower than the CH_4 selectivity for homogeneous reactions in empty reactor experiments. This could indicate that this sample is able to reform formed CH_4 to a larger extent than the other two samples.

The ethene selectivity is shown in Fig. 6. In this graph it is seen that the selectivity of ethene is increasing up to 800 °C for all of the catalytic materials. When the temperature has reached 800 °C the

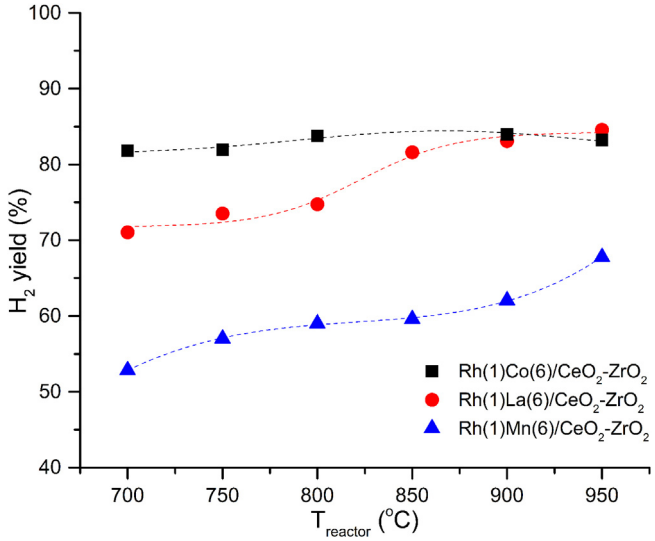

Fig. 4. H_2 yield for the three catalytic materials as a function of the reactor temperature. The operational parameters during the ATR experiments were GHSV ~ 50,000 h^{-1}, $H_2O/C \sim 2.5$ and $O_2/C \sim 0.45$. The numbers in parenthesis denote the nominal loading (wt.%) of Rh and promoters.

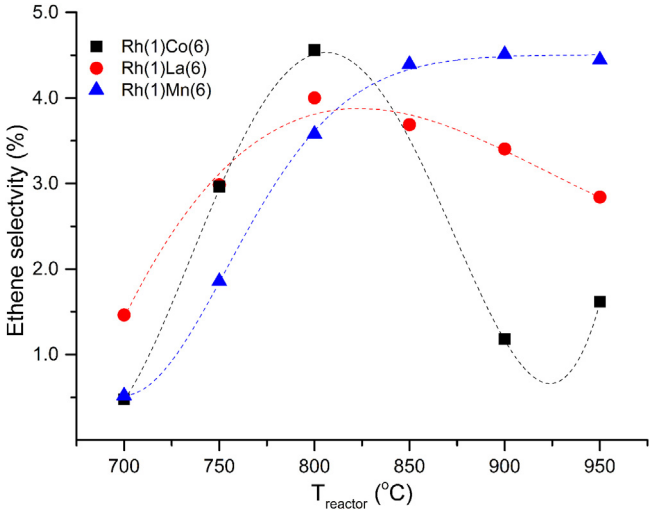

Fig. 6. Ethene selectivity for the three catalytic materials as a function of reactor temperature. The operational parameters during the ATR experiments were GHSV ~ 50,000 h^{-1}, $H_2O/C \sim 2.5$ and $O_2/C \sim 0.45$. The numbers in parenthesis denote the nominal loading (wt.%) of Rh and promoters.

behavior for ethene selectivity deviates between the samples. The selectivity for ethene levels out for the Rh/Mn sample meanwhile it decreases slowly for the Rh/La sample. The selectivity of ethene for the Rh/Co sample shows a peculiar behavior, drops sharp above 800 °C and increases again at 950 °C. This could have something to do with the fact that addition of cobalt increases the acidity of the support, which gives a potential increase in ethene formation. However, it has been seen that the Lewis sites of cobalt are highly active for C—C bond cleavage at lower temperatures [33].

The maximum selectivity for the light HCs, C_2 and C_3 (not reported), is generally between 750 °C and 850 °C, which is also the optimal ATR temperature range. The Rh/Mn catalyst is more prone to form higher HC (>C_2) than the other two catalytic materials. The Rh/La catalyst is the material with the least tendency to form higher HCs. This might be due to the fact that La_2O_3 increases the alkalinity of the already alkaline CeO_2-ZrO_2 and alkaline materials have proved to prevent coke formation [33]. The introduction of La_2O_3 in the CeO_2 matrix also increases the concentration of oxygen vacancies and the reducibility of the redox pair Ce^{4+}/Ce^{3+}, which seems to be an advantage in ATR of diesel [34].

Diesel slip is an important factor since it causes fuel penalty, deactivation of the following cleanup catalysts in the APU and is a poison to the fuel cell. The diesel slip for Rh/Co and Rh/La is around the same values above 750 °C and is completely eliminated above 800 °C. For the Rh/Mn catalyst, the diesel slip is more than four times higher at the lower temperatures and is eliminated around 850 °C, meaning that there is a high diesel slip for Rh/Mn in the desired operational temperature range.

5. Characterization results

5.1. BET specific surface area

The BET specific surface areas were measured both after the final calcination at 800 °C and after thermal treatment in air at 950 °C. The results are summarized in Table 1.

By comparing the loss in specific surface area for the La_2O_3-promoted sample and the support one can see that the percentage loss is less for the La_2O_3-promoted sample. It can be concluded that doping with La_2O_3 increases the thermal stability of CeO_2-ZrO_2. This improved thermal stability has been ascribed to the introduction of La_2O_3 in the CeO_2-ZrO_2 matrix, which causes a separation of cations at the grain boundaries, thus inhibiting the sintering of the material [34]. On the other hand promotion with Mn makes the catalytic material more sensitive to thermal treatment. The Rh/Mn sample loses almost 42% of its specific surface area during the thermal treatment.

The sample promoted with Co has the lowest specific surface area after both calcination and thermal treatment. The Rh/Co sample is also the sample with the highest activity of the evaluated materials. This indicates that specific surface area might not be one of the main characteristics important for a good ATR catalyst. It is also reasonable to argue that the main part of the reactions takes place primarily on the outer surface of the material or close to the pore mouth, due to the high reaction temperatures, implying that large specific surface areas might not be one of the key characteristics for ATR catalysts.

The average pore diameter of the Rh/Co sample after thermal treatment is considerably larger than for the other two samples. In fact it is twice as large as the average pore diameter for the Rh/La. It could be beneficial for ATR catalysts to have a larger average pore diameter since the diesel molecules are large and bulky. However, since there is no direct trend between catalytic activity and average pore diameter the parameter cannot be considered a key characteristic of the catalytic material for ATR.

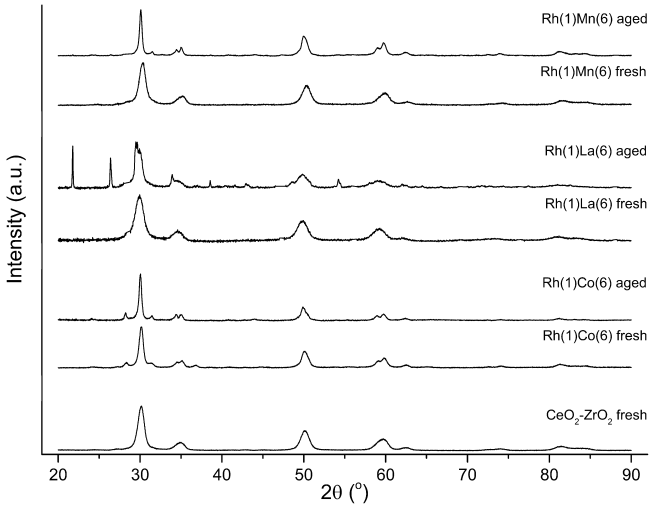

Fig. 7. XRD chromatograms of the fresh catalytic materials, aged catalytic materials and the support. The numbers in parenthesis denote the nominal loading (wt.%) of Rh and promoter.

5.2. X-ray powder diffraction

The X-ray powder diffractograms of the three fresh catalyst materials together with the support after the final calcination are shown in Fig. 7. In the X-ray diffractogram for CeO_2-ZrO_2, it is clear that the crystal phase of the calcined support is tetragonal, with the main peaks at 30.0°, 35.0°, 49.8°, and 59.6°.

Peaks that could be assigned to Rh species were not detected for any of the samples, the most reasonable explanation being that the amount is below the detection limit for the XRD instrument. For the samples promoted with La and Mn, no peaks could be found for the promoters. For the Rh/La sample, a plausible conclusion is that La_2O_3 replaces some of the CeO_2 in the ZrO_2 framework. This is possible because La^{3+} and Ce^{4+} have atomic radii close to each other. Separation of tetragonal CeO_2-ZrO_2 and tetragonal La_2O_3-ZrO_2 with XRD is hard due to the fact of very similar diffractograms. For the Rh/Mn sample, there is also a possibility that the Mn has dissolved in the matrix of the support. However, in this case it is more likely that the Mn ions fit in between the CeO_2 and ZrO_2 molecules rather than replacing them since the ionic radius is smaller than the ionic radii of both Zr^{4+} and Ce^{4+} [27]. For the sample promoted with Co, it was possible to identify peaks corresponding to the mixed Co-oxide, Co_3O_4.

By comparing the diffractogram of the fresh and aged samples some deviations are seen. One can see a separation of some peaks for the aged samples that are not visible for the fresh samples and depends on the different step size used in the XRD equipment used. Since the aged materials had to be scraped from the monolith there was a possibility of getting cordierite in the sample. This is clearly observed in the Rh/La aged sample where peaks of cordierite are visible at 21.7°, 26.4°, 33.9°, 38.5° and 54.3°. In the diffractogram of aged Rh/Mn sample there is a peak at 31.5° which is not visible for the fresh sample. This peak can be attributed to the presence of larger Mn_2O_3 crystals, caused by agglomeration of the Mn species of the catalyst.

The crystallite size for the identified species was calculated with the Scherrer formula and the values are summarized in Table 3. It can be seen that the size of the CeO_2-ZrO_2 crystals is considerably larger for the fresh Rh/Co sample than for the other two fresh samples. This is in line with the results from BET specific surface area measurements where it is significantly smaller than for the other samples. As seen in Table 3 the size of the detected Co-oxide crystals are close to the size of the CeO_2-ZrO_2 crystals. This means

Table 3
The average crystallite sizes for the catalytic materials estimated from the XRD diffractograms with the Scherrer formula. In the cases where no peaks for the species could be detected, the metal was assumed to be well dispersed and the crystals too small to detect with this technique.

Sample	Average particle sizes (nm)					
	Fresh samples			Aged samples		
	CeO_2-ZrO_2	Rh	Promoter	CeO_2-ZrO_2	Rh	Promoter
Rh(1)Co(6)[b]	14.3	n.a.	14.9	22.6	n.a.	30.0
Rh(1)La(6)[b]	7.2	n.a.	n.a.	9.2	n.a.	n.a.
Rh(1)Mn(6)[b]	9.7	n.a.	n.a.	24.9	n.a.	n.a.

[b] The numbers in parentheses are the nominal loading (wt.%) of Rh and promoters.

that a part of the Co_3O_4 is not supported on CeO_2-ZrO_2 but present as larger, unsupported crystals. In the results of the aged samples the behavior follows the one seen in the BET measurements for the thermally treated catalyst. It is see that the CeO_2-ZrO_2 crystals of the La-promoted sample are almost stable meanwhile the other two samples show a significant crystal growth. The stability of the La-promoted sample is most likely is due to the fact that La forms a protecting layer around the CeO_2-ZrO_2 particles, inhibiting the crystal growth [34]. The Co_3O_4 crystals have almost doubled in size compared to the fresh sample. This leads to considerably fewer active sites and a deactivation of the sample as consequence.

5.2.1. H_2-temperature programmed reduction

H_2-TPR measurements were performed on the fresh catalytic materials, the support and the support impregnated with one of Rh, Co, La or Mn. The resulting H_2-TPR profiles are shown in Fig. 8. The total H_2 uptake for each material was correlated to the total area underneath the H_2-TPR profiles. An overview of the total H_2 uptake for each sample is presented in Table 4.

The redox behavior of Ce_xO_2-$Zr_{(1-x)}O_2$ has been studied extensively over the years [35–37]. It is well-known that the H_2-TPR profile of pure CeO_2 consists of two distinct reduction peaks, which can be assigned to reduction of the surface and bulk oxygen, respectively [36]. By mixing CeO_2 with ZrO_2, the two reduction peaks are merged, to a different extent, depending on the ratio between species. The merging of the peaks is explained by the introduction of irregularities in the structure of CeO_2, enhancing the transport of bulk oxygen and lowering reduction temperature of bulk oxygen [20,38].

The H_2-TPR profile of CeO_2-ZrO_2 is shown in Fig. 8a together with the H_2-TPR profile of CeO_2-ZrO_2 impregnated with 1 wt.% Rh. In the profile for the sample impregnated with 1 wt.% Rh, the first peak, which appears below 200 °C, can be assigned to the reduction of Rh_2O_3 [39]. However, when the profile is deconvoluted mathematically, one can see that the peak consists of two merged peaks with maximum temperatures at 192 °C and 215 °C, respectively. Since the reduction of Rh_2O_3 takes place directly to Rh, the two peaks cannot be explained by the reduction of the Rh_2O_3 in two steps [40]. The explanation is rather a non-uniform size distribution of the Rh_2O_3 particles in the material [20,38]. The small, well-dispersed particles are reduced at the temperature corresponding to the first peak, while the reduction temperature of the larger, more bulk-like crystalline Rh_2O_3 particles corresponds to the second peak. Previous work has pointed out that the Rh particles are less dispersed when supported on CeO_2-ZrO_2 than when supported on pure CeO_2 [20]. This coherent peak for the reduction of Rh_2O_3 is not seen in the H_2-TPR profiles of the catalytic materials, leading to the conclusion that the size distribution of Rh_2O_3 is more uniform when one of the promoters is present in the material.

By comparing the H_2 uptake for the support and the support impregnated with 1 wt.% Rh in Table 4 one can see an expected increase in the H_2 uptake. However the increase is too large to be explained not only by the Rh_2O_3 reduction alone. The explanation for the larger part of this increase is that the reducibility of CeO_2 is increased in the present of PGM metals [17]. In Fig. 8a, it can be seen that the presence of Rh_2O_3 not only increases the reducibility but also reduces the reduction temperature for CeO_2.

The two samples promoted with Co_3O_4 exhibit much higher H_2 uptake than the other materials. The H_2-TPR profile of CeO_2-ZrO_2 impregnated with cobalt exhibits two clear peaks, which are believed to correspond to the reduction of Co_3O_4, which is a mixed oxide consisting of Co_2O_3 and CoO. The two more diffuse peaks probably belong to the reduction of Ce_2O_3, which is slightly enhanced and also lowered in temperature by the addition of Co_3O_4. By adding Rh to the sample, the H_2-TPR profile changes considerably. The addition of Rh increases the reducibility of both Co_3O_4 and Ce_2O_3 and the material is close to fully reduced below 600 °C. The increased reducibility of both cobalt and ceria when Rh is added is in line with what others have observed [29]. This would mean that both Rh and Co are in their metallic state in the Rh/Co sample over the evaluated temperature range. It also implies that most of the CeO_2 is reduced. However, in the oxidizing environment at the front of the monolith, most of the Ce_2O_3 is reduced and one possible explanation for Rh/Co having such high activity might be that the oxygen can be stored at the front of the monolith and transported to the end of the catalyst, which makes the oxidative zone longer and the temperature higher for the steam reforming part.

When CeO_2-ZrO_2 is promoted with La_2O_3 the H_2 uptake decreases compared to CeO_2-ZrO_2. This result is in line with what other have observed [41]. On the contrary addition of La_2O_3 has proven to enhance the redox cycling of other involved species [42]. However, the H_2-TPR profile for the Rh/La sample is similar to the H_2-TPR profile of the 1 wt.% Rh sample and the H_2 uptake for the two samples is close to each other.

The increase in H_2 uptake between CeO_2-ZrO_2 and the sample impregnated with 6 wt.% Mn corresponds to the H_2 uptake for reducing the Mn_2O_3. The reduction temperature of CeO_2 is also not affected by the addition of Mn_2O_3. However when adding Rh to the sample the reduction temperatures of both Mn_2O_3 and CeO_2 are decreased. This is evidence of a synergistic interaction between Mn_2O_3 and CeO_2, causing the reduction of Mn_2O_3 at a lower temperature compared to unsupported Mn oxide [43]. On the other

Table 4
The measured total H_2 uptake for the catalytic materials compared with the H_2 uptake for the support, Rh(1)/CeO_2-ZrO_2, Co(6)/CeO_2-ZrO_2, La(6)/CeO_2-ZrO_2 and Mn(6)/CeO_2-ZrO_2. The H_2-TPR profiles are presented in Fig.8.

Sample	Total H_2 uptake (μmol/g)
CeO_2-ZrO_2	2505
Rh(1)[b]	3011
Co(6)[b]	6365
Rh(1)Co(6)[b]	8575
La(6)[b]	1990
Rh(1)La(6)[b]	3061
Mn(6)[b]	3596
Rh(1)Mn(6)[b]	4419

[b] The numbers in parentheses are the nominal loading (wt.%) of Rh and promoters.

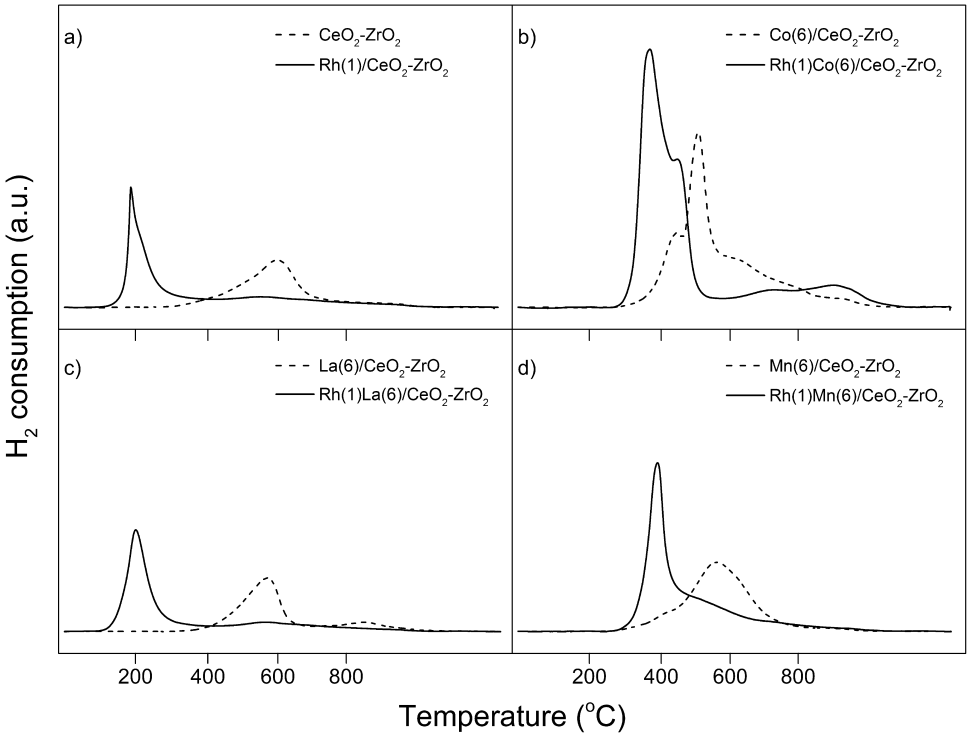

Fig. 8. H_2-TPR profiles for the fresh catalytic materials, the support and the support impregnated with promoters; (a) CeO_2-ZrO_2 and Rh(1)/CeO_2-ZrO_2, (b) Co(6)/CeO_2-ZrO_2 and Rh(1)Co(6)/CeO_2-ZrO_2 (c) La(6)/CeO_2-ZrO_2 and Rh(1)La(6)/CeO_2-ZrO_2 and (d) Mn(6)/CeO_2-ZrO_2 and Rh(1)Mn(6)/CeO_2-ZrO_2. The numbers in parenthesis denote the nominal loading (wt.%) of Rh and promoters.

hand, the combination of Rh and Mn increases the reduction temperature for Rh. The small reduction shoulder below 400 °C on the Mn sample corresponds to small, well-dispersed particles of Mn being reduced at a lower temperature. The reduction of Mn_2O_3 is similar to the bulk reduction of Mn, which leads to the conclusion that Mn oxides consist mainly of microcrystalline material [44].

6. Conclusions

This evaluation shows that it is possible to lower the amount of Rh content in catalysts for ATR of diesel without compromising the activity. In the study the three different catalysts (1 wt.% Rh/6 wt. X (X = Co, La, Mn)/CeO_2-ZrO_2 showed comparable catalytic activity as a 3 wt.% Rh/CeO_2-ZrO_2 catalyst previously tested in our laboratory [19]. However the combination of Rh/Co showed a superior activity and H_2 yield over the evaluated temperature range. Another interesting finding is that the combination of Rh/La results in very low selectivity towards HC, which is beneficial from a coking perspective.

Other interesting things were; that both Rh/Co and Rh/La samples have low diesel slip in the optimal temperature range for ATR of diesel. Additionally, the CH_4 selectivity for the Rh/Mn sample was temperature independent. It seems like it is beneficial to increase the reducibility of CeO_2 in order to obtain a more active catalytic material for ATR of diesel.

The La-promoted sample shows a very high resistance toward sintering. Both the BET measurements and the XRD measurements show very little changes in the specific surface area and the crystal sizes of CeO_2-ZrO_2.

Acknowledgements

The Swedish Foundation for Strategic Environmental Research (Mistra) is gratefully acknowledged for financial support. The financial support from KIC InnoEnergy in the project SynCon is also gratefully acknowledged. Thanks to MEL Chemicals for providing the CeO_2-ZrO_2 support, Corning Inc. for supplying the cordierite monoliths and Neste Oil, Finland for supplying the NExBTL biodiesel. Thanks also to KIT for the help with the diesel vaporization system in the miniature reactor setup at KTH [45].

References

[1] H. Kannisto, X. Karatzas, J. Edvardsson, L.J. Pettersson, H.H. Ingelsten, Appl. Catal. B: Environ. 104 (2011) 78–83.
[2] D.J. Liu, T.D. Kaun, H.K. Liao, S. Ahmed, Int. J. Hydrogen Energy 29 (2004) 1035–1046.
[3] United States Environmental Protection Agency (EPA), www.epa.gov (visited: 20-01-14).
[4] M. Contestabile, Energy Policy 38 (2010) 5320–5334.
[5] S.M.A. Rahman, H.H. Masjuki, M.A. Kalam, M.J. Abedin, A. Sanjid, H. Sajjad, Energy Convers. Manage. 74 (2013) 171–182.
[6] N. Lutsey, C.-J. Brodrick, T. Lipman, Energy 32 (2007) 2428–2438.
[7] DieselNet, www.dieselnet.com (visited: 25-01-2014).
[8] F. Baratto, U.M. Diwekar, J. Power Sources 139 (2005) 188–196.
[9] P. Agnolucci, W. McDowall, Technol. Forecast. Social Change 74 (2007) 1394–1410.
[10] B. Sakintuna, F. Lamari-Darkrim, M. Hirscher, Int. J. Hydrogen Energy 32 (2007) 1121–1140.
[11] S. Specchia, V. Specchia, Ind. Eng. Chem. Res. 49 (2010) 6803–6809.
[12] D.J. Haynes, A. Campos, D.A. Berry, D. Shekhawat, A. Roy, J.J. Spivey, Catal. Today 155 (2010) 84–91.
[13] G. Kolb, Chem. Eng. Process. 65 (2013) 1–44.
[14] A. Cutillo, S. Specchia, M. Antonini, G. Saracco, V. Specchia, J. Power Sources 154 (2006) 379–385.
[15] D.J. Haynes, D. Shekhawat, in: D. Shekhawat, J.J. Spivey, D. Berry (Eds.), Fuel Cells: Technologies for Fuel Processing, Elsevier Science, Amsterdam, 2011.
[16] A.B. Stiles, Catalyst Supports and Supported Catalysts: Theoretical and Applied Concepts, Butterworths, Boston, 1987.
[17] H.C. Yao, Y.F.Y. Yao, J. Catal. 86 (1984) 254–256.
[18] X. Karatzas, K. Jansson, A. González, J. Dawody, L.J. Pettersson, Appl. Catal. B: Environ. 106 (2011) 476–487.
[19] M. Nilsson, Hydrogen Generation for Fuel Cells in Auxiliary Power Systems, PhD thesis, KTH Royal Institute of Technology, Stockholm, 2009.
[20] C. Diagne, H. Idriss, A. Kiennemann, Catal. Commun. 3 (2002) 565–571.
[21] R.D. Monte, J. Kaspar, J. Mater. Chem. 15 (2005) 633–648.

[22] S. Specchia, E. Finocchio, G. Busca, P. Palmisano, V. Specchia, J. Catal. 263 (2009) 134–145.
[23] H.R. Pouretedal, Z. Tofangsazi, M.H. Keshavarz, J. Alloys Compd. 513 (2012) 359–364.
[24] J. Wang, W. Xu, L. Chen, Y. Jia, L. Wang, X.-J. Huang, J. Liu, Chem. Eng. J. 231 (2013) 198–205.
[25] Platinum Today, www.platinum.matthey.com (visited: 23-11-13).
[26] Y.-F. Chang, J.G. McCarty, Catal. Today 30 (1996) 163–170.
[27] A. Bampenrat, V. Meeyoo, B. Kitiyanan, P. Rangsunvigit, T. Rirksomboon, Appl. Catal. A: Gen. 373 (2010) 154–159.
[28] N. Laosiripojana, W. Sutthisripok, P. Kim-Lohsoontorn, S. Assabumrungrat, Int. J. Hydrogen Energy 35 (2010) 6747–6756.
[29] L.M.T. Martínez, M. Araque, J.C. Vargas, A.C. Roger, Appl. Catal. B: Environ. 132–133 (2013) 499–510.
[30] X. Karatzas, J. Dawody, A. Grant, E.E. Svensson, L.J. Pettersson, Appl. Catal. B: Environ. 101 (2011) 226–238.
[31] P.K. Cheekatamarla, A.M. Lane, J. Power Sources 152 (2005) 256–263.
[32] M. Hartmann, L. Maier, H.D. Minh, O. Deutschmann, Combust. Flame 157 (2010) 1771–1782.
[33] J.S. Moura, M.O.G. Souza, J.D.A. Bellido, E.M. Assaf, M. Opportus, P.M. Reyes, d.C. Rangel, Int. J. Hydrogen Energy 37 (2012) 3213–3224.
[34] W.Y. Hernández, O.H. Laguna, M.A. Centeno, J.A. Odriozola, J. Solid State Chem. 184 (2011) 3014–3020.
[35] M.D. Salazar-Villalpando, D.A. Berry, T.H. Gardner, Int. J. Hydrogen Energy 33 (2008) 2695–2703.
[36] G. Balducci, P. Fornasiero, R. Monte, J. Kaspar, S. Meriani, M. Graziani, Catal. Lett. 33 (1995) 193–200.
[37] P. Fornasiero, G. Balducci, R. Di Monte, J. Kašpar, V. Sergo, G. Gubitosa, A. Ferrero, M. Graziani, J. Catal. 164 (1996) 173–183.
[38] L. Cao, L. Pan, C. Ni, Z. Yuan, S. Wang, Fuel Process. Technol. 91 (2010) 306–312.
[39] J.A. Wang, T. López, X. Bokhimi, O. Novaro, J. Mol. Catal. A: Chem. 239 (2005) 249–256.
[40] C. Padeste, N. Cant, D. Trimm, Catal. Lett. 28 (1994) 301–311.
[41] L.N. Ikryannikova, A.A. Aksenov, G.L. Markaryan, G.P. Murav'eva, B.G. Kostyuk, A.N. Kharlanov, E.V. Lunina, Appl. Catal. A: Gen. 210 (2001) 225–235.
[42] X.-Y. Jiang, R.-X. Zhou, P. Pan, B. Zhu, X.-X. Yuan, X.-M. Zheng, Appl. Catal. A: Gen. 150 (1997) 131–141.
[43] L. Jia, M. Shen, J. Hao, T. Rao, J. Wang, J. Alloys Compd. 454 (2008) 321–326.
[44] F. Kapteijn, A.D. Vanlangeveld, J.A. Moulijn, A. Andreini, M.A. Vuurman, A.M. Turek, J.M. Jehng, I.E. Wachs, J. Catal. 150 (1994) 94–104.
[45] Institute for Micro Process Engineering, Karlsruhe Institute of Technology, www.imvt.kit.edu (visited: 02-11-2013).
[46] Svenska petroleum & biodrivmedel institutet, www.spbi.se (visited: 06-11-13).
[47] Neste Oil, www.nesteoil.com (visited: 17-02-14).